Carbohydrate Research, 230 (1992) 223–244
Elsevier Science Publishers B.V., Amsterdam

Conformational analysis of the anomeric forms of kojibiose, nigerose, and maltose using MM3

Michael K. Dowd [a], Jing Zeng [a], Alfred D. French [b] and Peter J. Reilly [a]

[a] *Department of Chemical Engineering, Iowa State University, Ames, Iowa 50011 (USA)*
[b] *Southern Regional Research Center, U.S. Department of Agriculture, New Orleans, Louisiana 70179 (USA)*

(Received October 28th, 1991; accepted December 30th, 1991)

ABSTRACT

Energy surfaces were computed for relative orientations of the relaxed pyranosyl rings of the two anomeric forms of kojibiose, nigerose, and maltose, the (1 → 2)-α-, (1 → 3)-α-, and (1 → 4)-α-linked D-glucosyl disaccharides, respectively. Twenty-four combinations of starting conformations of the rotatable side-groups were considered for each disaccharide. Optimized structures were calculated using MM3 on a 20° grid spacing of the torsional angles about the glycosidic bonds. The energy surfaces of the six disaccharides were similar in many respects but differed in detail within the low-energy regions. The maps also illustrate the importance of the exo-anomeric effect and linkage type in determining the conformational flexibility of disaccharides. Torsional conformations of known crystal structures of maltosyl-containing molecules lie in a lower MM3 energy range than previously reported.

INTRODUCTION

Recent hardware and software advances have enabled the generation of relaxed-residue or adiabatic energy maps for studying carbohydrate conformations. Several papers have been presented on maltose[1–4] and cellobiose[3,5–7], but little work has appeared for the other α- and β-linked D-glucosyl disaccharides. Not since the early investigations of Sathyanarayana and Rao[8,9] of both α- and β-linked D-glucosyl disaccharides has there been a study to compare the conformational similarities and differences caused by the point of attachment of the glycosidic linkage to the reducing saccharide ring. They showed with rigid monomer techniques that the global minimum for maltose existed in a different conformer region than those for nigerose and kojibiose. Presented here is a comparison of relaxed-residue computational analyses of kojibiose [α-D-glucopyranosyl-(1 → 2)-D-glucose (**1**), Fig. 1], nigerose [α-D-glucopyranosyl-(1 → 3)-D-glucose (**2**)], and maltose [α-D-glucopyranosyl-(1 → 4)-D-glucose (**3**)], all having their glycosidic linkages

Correspondence to: Dr. P.J. Reilly, Department of Chemical Engineering, Iowa State University, Ames, IA 50011, USA.

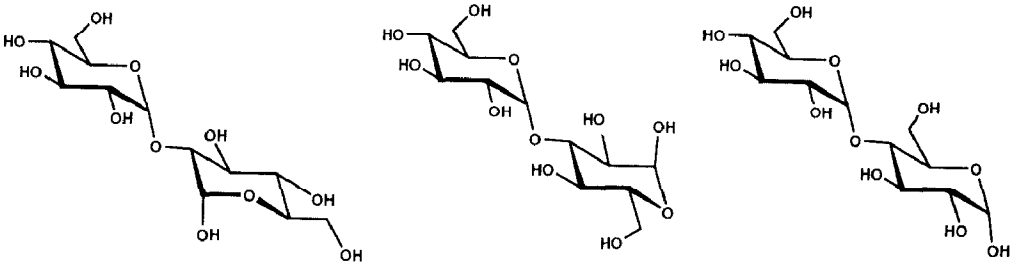

1 2 3

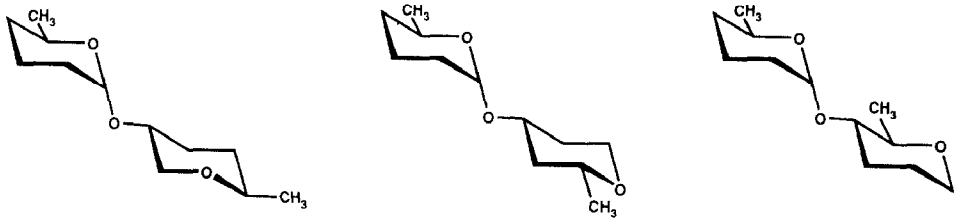

4 5 6

Fig. 1. Molecular structures of α-kojibiose (**1**), α-nigerose (**2**), α-maltose (**3**), axially–equatorially linked 3-(6-methyltetrahydropyran-2-yloxy)-6-methyltetrahydropyran (**4**), axially–equatorially linked 4-(6-methyltetrahydropyran-2-yloxy)-6-methyltetrahydropyran (**5**), and axially–equatorially linked 5-(6-methyltetrahydropyran-2-yloxy)-6-methyltetrahydropyran (**6**).

axial to the plane of the ring for the nonreducing residue and equatorial to the plane of the ring for the reducing residue. Anomeric forms of the reducing rings, which have not previously been compared within a single study, are also considered. Numerous crystal structures are known for maltose and maltosyl-containing molecules, and a comparison of MM3-generated low-energy conformations with these structures is made. The MM3 map for maltose is compared with similar maps generated with other molecular mechanics algorithms.

COMPUTATIONAL METHODS

The torsional angles representing the orientations of the rings about the glycosidic bonds are defined as ϕ = H-1–C-1–O-1–C-i' and ψ = C-1–O-1–C-i'–H-i' (Fig. 2), where $i' = 2$, 3, or 4, depending on the disaccharide studied. The computational procedure for generating ϕ, ψ steric energy maps is an extension of that presented by French et al.[7]. It was implemented for a UNIX system and has been previously described[10]. The force field used in this study was MM3 (January 22, 1990 update) developed by Allinger[11–13] and marketed by the Technical Utilization Corporation, Powell, OH. This potential function is the successor of the

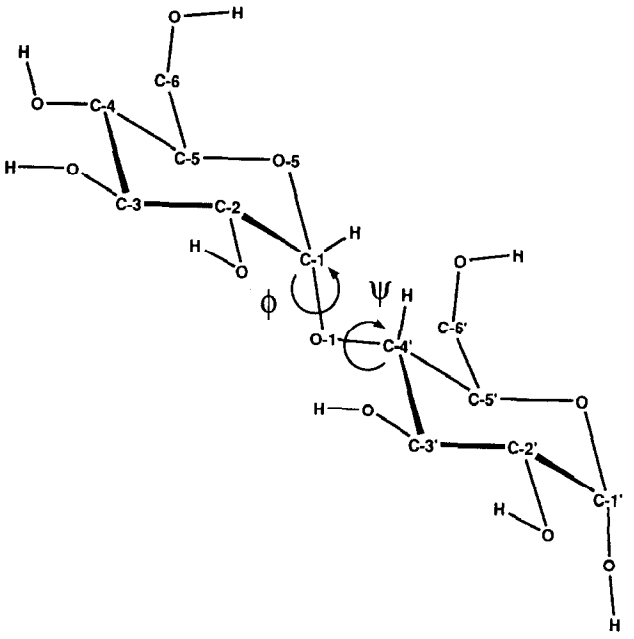

Fig. 2. Definition of the torsional angles ϕ and ψ in α-maltose. For both rings the hydroxymethyl groups are oriented *gauche–gauche* to C-4 and O-5 and the secondary hydroxyls are in a clockwise arrangement around the rings (i.e., *ggggcc*).

widely used MM2 series of programs[14], which have been favorably compared with other molecular mechanics models and with semi-empirical methods[15], and which have been used extensively for the study of carbohydrate structures[2–7]. The MM3 dielectric constant (ε) was set to 4.0 for all calculations, as has been found most appropriate from studies of the D-glucopyranose ring in comparison with crystal structures[16]. The block diagonal minimization method, with a default convergence criterion of 3.6 cal/mol, was used for grid-point optimizations. All maps were constructed with 20° grid spacing except where noted.

Twenty-four starting conformers of each disaccharide were generated using PC-Model (Serena Software, Bloomington, ID). The initial structures consisted of $^4C_1$ D-glucopyranosyl ring conformers with either *gauche–gauche* (*gg*) or *gauche–trans* (*gt*) orientations of the hydroxymethyl groups (relative to the ring O-5 and C-4 atoms, respectively) and with the hydroxyl hydrogen atoms oriented to form potential hydrogen bonds with the ring oxygen atoms. The *tg* forms were neglected, since they have higher MM3 energies at $\varepsilon = 4.0$ (work in progress on D-glucopyranosyl rings), and are not found in crystal structures[17] or as significant conformers in solution[18–19]. Ha et al.[1] considered clockwise (*c*) and reverse-clockwise (*r*) orientations of the secondary hydroxyl groups that form a partial hydrogen bonding ring around the pyranose ring and discussed the evidence for the existence of such structures. The same idea is exploited here to account for the secondary hydroxyls. Two reverse-clockwise orientations, *r* and *r'*, are considered,

TABLE I

Approximate (±5°) angles used for clockwise (*c*) and reverse-clockwise (*r* and *r'*) torsional orientations of the secondary hydroxyl groups of kojibiose, nigerose, and maltose

Torsional angle	α Anomer			β Anomer		
	c	*r*	*r'*	*c*	*r*	*r'*
Nonreducing ring						
H(O-2)–O-2–C-2–C-3	−60	180	60	−60	180	60
H(O-3)–O-3–C-3–C-4	60	180	180	60	180	180
H(O-4)–O-4–C-4–C-5	−60	180	180	−60	180	180
Reducing ring						
H(O-1')–O-1'–C-1'–C-2'	−60		180	60	180	
H(O-2')–O-2'–C-2'–C-3' [a]	−60		60	−60	180	
H(O-3')–O-3'–C-3'–C-4' [b]	60		180	60	180	
H(O-4')–O-4'–C-4'–C-5' [c]	−60		180	−60	180	

[a] Not applicable for kojibiose. For this disaccharide, *r* and *r'* are identical conformations when referenced to the reducing ring. [b] Not applicable for nigerose. [c] Not applicable for maltose.

with the C-3–C-2–O-2–H(O-2) torsional angle being 180° for the *r* orientation and 60° for the *r'* orientation. The 180° orientation is favorable for continuing the hydrogen bond ring from C-2 to C-1 when the glycosidic oxygen atom is equatorially aligned (on the reducing ring of a β anomer), while the 60° orientation is favorable when the glycosidic oxygen atom is axially aligned (on the reducing ring of an α anomer and for the nonreducing ring of α-linked disaccharides). In addition, since for the nonreducing ring the 180° angle for C-3–C-2–O-2–H(O-2) is a favorable orientation for forming a possible inter-ring hydrogen bond with the reducing ring, the *r* conformation for the nonreducing ring was also studied. In summary, three secondary hydroxyl orientations (*c*, *r*, and *r'*) were considered for the nonreducing ring and two (either *c* and *r*, or *c* and *r'*, depending on the anomeric form) were considered for the reducing ring. The starting orientations of these torsional angles are defined in Table I. These six orientations of the secondary hydroxyls combined with the four hydroxymethyl orientations yield the 24 starting conformations.

The lowest energy value from the 24 optimized starting conformers was used at each grid-point to construct the energy maps. Isoenergy contour lines were generated using the routines available within DISSPLA Graphics, Release 11.0 (Computer Associates International, Garden City, NY). In effect, the ϕ,ψ maps represent a two-dimensional projection from a hyperenergy space of many dimensions. Complete grids from −180 to +180° were calculated. Consequently, one row and one column of overlapping grid-points were calculated in completing the grid. Occasionally different starting conformers with nearly identical energies yielded the final points at these equivalent positions. There are two possibly interrelated reasons for this occurrence. First, the MM3 driver procedure of restricting torsional movement by invoking large rotational barriers, coupled with small deviations in the starting structures after the initial rotations, can result in

slightly different energy values for the normally identical 180 and −180° conformations. Second, different starting structures may be optimized to the same effective final conformation with similar energies. The final map grid-points were not checked for retention of the conformational characteristics of the starting structure, since this would require retaining all of the grid-point structures.

For each local low-energy region of a map, the starting conformer (*ggggcc*, etc.) that contributed the lowest energy grid-point and the eight nearest neighbor conformers, if different, were rotated with the MM3 driver option to this grid-point location, followed by nonrestricted minimization to the optimal local structure. The MM3 block-diagonal followed by full-matrix optimization method (MM3 Option 2) was used to isolate all local minima. Full-matrix optimization yielded energies 0.1 to 0.2 kcal/mol lower for the calculated minima than did the block-diagonal method. In general, the starting conformer that contributed the lowest energy grid-point also yielded the local minimum. Energy values of these minima were typically 0.2 to 0.4 kcal/mol less than the lowest energy grid-point. The final locations of minima were found within the local regions, although they could be several degrees removed from the grid-point structure. Occasionally, these minima were displaced outside the nearest contour line, presumably because of the interpretive nature of developing contours from data based on a fixed grid-spacing. Areas that exhibited low-energy gradients or plateaus were also checked, as energy minima were found in these regions on an α,α-trehalose map[10]. For these points the final minimum was checked by optimization of the nearest neighbor starting conformers at the final ϕ,ψ location in order to ensure that structures not yielding a local minimum did not have lower energies at these points. Minima in these regions are reported only if the full-matrix method produced an optimized minimum within the local region.

One estimate of glycosidic conformational freedom is the percentage of adiabatic map space occupied within a specified range of the global energy minimum. This area can be approximated by summing the number of grid-points that fall within the outlined region, but this measure suffers in the severe weighting of the individual conformers [either 0 (excluded) or 1 (included)]. By considering the individual energies associated with different ϕ,ψ conformational states, a conformational partition function that accounts for different ϕ,ψ conformational states provides a more rigorous method for estimating of the conformational freedom of the glycosidic linkage. For this purpose q is defined as

$$q = \sum_{\phi,\psi} \exp[-E(\phi,\psi)/RT]$$

where $E(\phi,\psi)$ is the Boltzmann-averaged energy calculated from the optimized 24 starting conformers, R is the gas constant, and T is the temperature. Although only a small portion of the conformational space was sampled in estimating $E(\phi,\psi)$, the starting conformations considered are believed to be at the lowest energy and hence to contribute the most to this average. Based on this partition

function, an average disaccharide energy can be calculated from

$$E_{av} = \sum_{\phi,\psi} \frac{E(\phi,\psi)\ \exp(-E(\phi,\psi)/RT)}{q}$$

For all calculations, a temperature of 298.2 K was used.

Conformational maps were also generated for the 6-methyltetrahydropyran analogues of kojibiose, nigerose, and maltose [axially–equatorially linked 3-(6-methyltetrahydropyran-2-yloxy)-6-methyltetrahydropyran (**4**), Fig. 1, axially–equatorially linked 4-(6-methyltetrahydropyran-2-yloxy)-6-methyltetrahydropyran (**5**), and axially–equatorially linked 5-(6-methyltetrahydropyran-2-yloxy)-6-methyltetrahydropyran (**6**), respectively]. Similar analogues have been used as carbohydrate models in past computational studies[10,20]. These analogues have no hydroxyl groups, eliminating the need to consider multiple starting conformers, and therefore the maps were constructed with 10° grid-spacing. The $^5C_2$ tetrahydropyran chair conformation, equivalent to the $^4C_1$ pyranose conformation found in D-glucosyl rings, was used as the starting ring conformation for these analogues.

RESULTS

α- and *β*-Kojibiose.—The MM3-generated maps of *α*- and *β*-kojibiose are shown in Fig. 3. The substantial differences in the maps must be related to the positioning of the anomeric hydroxyl group. As this groups is adjacent to the glycosidic linkage, and hence to the other ring, differences caused by anomeric orientations should be more pronounced for kojibiose than for nigerose and maltose. A deep trough of low-energy conformations, running in the *ψ*-direction

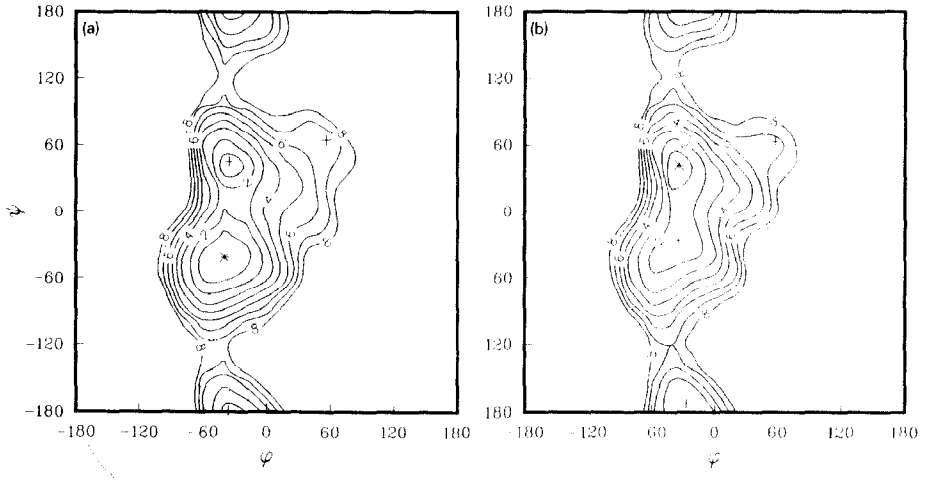

Fig. 3. MM3-generated relaxed-residue steric energy maps of *α*-kojibiose (a) and *β*-kojibiose (b). Contour lines are graduated in 1 kcal/mol increments above the global minimum: (*) global minimum; (+) other minima.

TABLE II

Steric energy minima for MM3-generated relaxed-residue analysis of kojibiose, nigerose, and maltose

Disaccharide	Location of minimum		Initial conformer	Relaxed energy (kcal/mol)
	ϕ	ψ		
α-Kojibiose	−39.4	−41.2	*gtgtr'r'*	21.53
	−35.1	45.6	*gtgtrr'*	21.68
	−35.9	−178.5	*gtgtrr'*	25.12
	56.0	64.9	*gtggr'c*	27.63
β-Kojibiose	−33.8	42.0	*gtgtr'r*	20.78
	−34.7	−26.4	*gtgtr'r*	22.23
	−27.1	−172.1	*gtgtcr*	24.64
	57.5	63.1	*gtgtrc*	27.45
α-Nigerose	−34.8	47.4	*gtgtr'c*	21.62
	−24.0	−19.4	*gtgtcc*	22.76
	−25.4	−171.5	*gtgtr'r'*	25.13
β-Nigerose	−36.0	46.3	*gtgtr'c*	21.42
	−35.2	−2.0	*gtgtcr*	22.19
	−23.0	−173.6	*gtgtcc*	24.47
	57.0	63.3	*gtgtrr*	26.22
α-Maltose	−22.7	−21.7	*gtggcc*	22.74
	−54.6	−47.5	*gtgtr'r'*	22.99
	−30.6	−167.8	*gtgtrc*	24.35
β-Maltose	−54.3	−47.4	*gtgtr'r*	22.05
	−28.3	−27.5	*gtggrr*	22.22
	0.6	23.7	*gtgtr'r*	24.09
	−28.0	−170.5	*gtgtrc*	24.74

and centered about a staggered conformation between ϕ values of −60 and 0°, occurs in both α- and β-kojibiose. The four minima for each anomer, the three lowest of which are centered in this trough, are listed in Table II, along with their steric energy values. For α-kojibiose the global minimum is located at $\phi,\psi = -39, -41°$, while the second minimum is at $\phi,\psi = -36,46°$. An energy difference of just 0.15 kcal/mol exists between these two minima. An interring hydrogen bond is formed between O-5 and H(O-3′) for the minimum near $\psi = 50°$. For β-kojibiose the relative placement of the two lowest minima is reversed, with the global minimum occurring at $\phi,\psi = -34,42°$ and the second minimum occurring at $\phi, \psi = -35, -26°$. The same inter-ring hydrogen bond found in the second minimum of α-kojibiose is present in the global minimum of β-kojibiose. In both anomers the oxygen-to-hydrogen distance of this bond is 0.1944 nm. Table III presents selected geometric parameters about the glycosidic linkages for the two global minima. Few large differences exist between the anomeric forms except for the torsional angles. Two additional minima with relatively high energies are present on each map (Table II). One of these exists at a staggered orientation, with ψ close to 180°. The other is in a shallow depression with each of the glycosidic torsional

TABLE III

Selected MM3-generated bond lengths, valence angles, and torsional angles for the global minima of α- and β-kojibiose

Bonds	α-Kojibiose	β-Kojibiose
	Bond lengths (nm)	
C-1–C-2	0.1527	0.1527
C-1–O-1	0.1419	0.1418
C-1–O-5	0.1422	0.1422
C-5–O-5	0.1425	0.1426
C-1′–C-2′	0.1531	0.1530
C-1′–O-1′	0.1431	0.1421
C-1′–O-5′	0.1419	0.1425
C-2′–C-3′	0.1528	0.1533
C-2′–O-1	0.1426	0.1427
C-5′–O-5′	0.1424	0.1422
	Valence angles (degrees)	
C-1–O-1–C-2′	114.5	115.9
C-1–O-5–C-5	115.0	114.9
C-2–C-1–O-1	108.4	108.3
C-2–C-1–O-5	109.3	108.9
O-1–C-1–O-5	111.0	111.3
C-1′–C-2′–O-1	109.3	105.0
C-1′–C-2′–C-3′	110.5	109.7
C-1′–O-5′–C-5′	114.9	112.4
C-2′–C-1′–O-1′	109.7	107.5
C-2′–C-1′–O-5′	109.6	109.3
C-3′–C-2′–O-1	107.3	110.1
O-1′–C-1′–O-5′	110.7	107.9
	Torsional angles (degrees)	
H-1–C-1–O-1–C-2′	−39.4	−33.8
C-1–O-1–C-2′–H-2′	−41.2	42.0
C-1–O-1–C-2′–C-1′	79.9	160.4
C-1–O-1–C-2′–C-3′	−160.2	−81.6
C-2–C-1–O-1–C-2′	−158.2	−152.5
C-2–C-1–O-5–C-5	−58.7	−59.4
C-5–O-5–C-1–O-1	60.9	60.0
O-5–C-1–O-1–C-2′	81.8	87.8

angles in a staggered position, with ϕ,ψ values near 60°. Although the exo-anomeric effect works against the staggered orientation of ϕ near 60°, minima in this region of the ϕ,ψ map have been found for other disaccharides[21,22]. The Boltzmann-averaged energy of β-kojibiose is lower (Table IV). Anomeric ratios have been reported for disaccharides based on NMR spectroscopy[23] and by gas–liquid chromatography after preventing mutarotation by derivatization of the hydroxyl groups[24–26]. Although solvation effects have not been considered in this study, the relative MM3 energies are in agreement with the experimental anomeric distribution of kojibiose in pyridine[26] and water[24,25]. The early NMR report found α-kojibiose in deuterium oxide to be of slightly higher concentration than β-kojibiose[23].

TABLE IV

Molecular partition function (q) and Boltzmann-averaged MM3 energy for axially–equatorially linked disaccharides

Disaccharide	q	Average energy (kcal/mol)
α-Kojibiose	4.3	22.99
β-Kojibiose	2.1	22.71
α-Nigerose	4.4	23.45
β-Nigerose	5.5	23.12
α-Maltose	4.0	23.98
β-Maltose	5.3	23.31

Several initial conformers are represented on each of the final maps (Fig. 4). The orientation of the anomeric hydroxyl appears to have only a minor influence on the distribution of starting conformers contributing to the low-energy region. For each anomer, the starting conformers with the *gtgt* orientation of the hydroxymethyl groups yield more than 80% of the final map points (Table V), with the most important individual contributors being the *gtgtr'r'* conformation for α-kojibiose and *gtgtr'r* conformation for β-kojibiose. The *gt* orientation also yields a lower MM3 energy than the *gg* orientation for the D-glucopyranosyl ring (work in progress). The 8 kcal/mol contour line surrounds a larger region of the ϕ,ψ map for α-kojibiose, which suggests that this form has slightly more conformational freedom about its glycosidic bonds. The partition function calculation suggests the

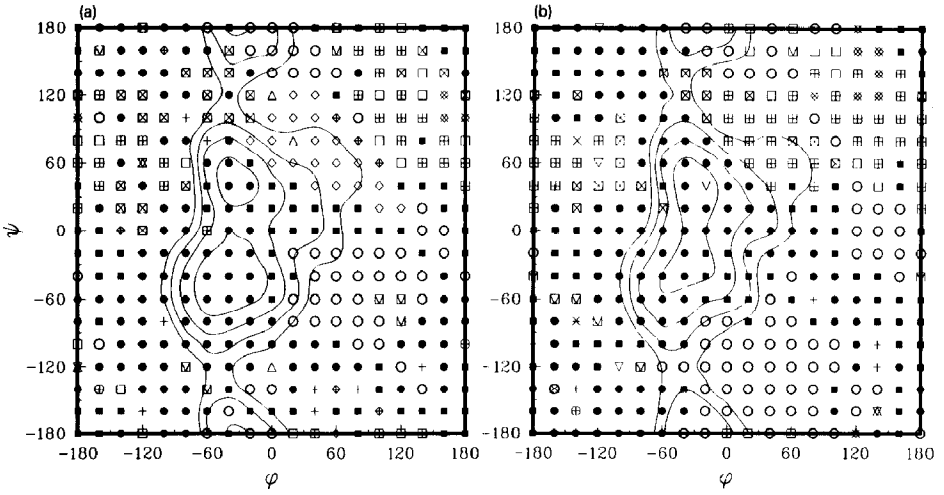

Fig. 4. Distribution of the starting conformers that contribute to the final relaxed-residue maps of α-kojibiose (a) and β-kojibiose (b). Starting conformers are: *ggggrx* (⊗); *gggtcc* (⊠); *gggtcx* (⊡); *gggtr'x* (+); *gggtrc* (×); *gggtrx* (∗); *gtggcc* (⊕); *gtggcx* (⊠); *gtggr'c* (⊕); *gtggr'x* (▽); *gtggrc* (◇); *gtggrx* (△); *gtgtcc* (□); *gtgtcx* (○); *gtgtr'c* (⊠); *gtgtr'x* (●); *gtgtrc* (⊞); *gtgtrx* (■). For the reducing ring secondary hydroxyl orientation, x represents r' for α-kojibiose and r for β-kojibiose. Contour lines are graduated in 2 kcal/mol increments above the overall energy minimum.

TABLE V

Starting structures contributing to MM3-generated relaxed-residue ϕ, ψ disaccharide maps

Disaccharide	Complete map		Lowest 8 kcal/mol		
	Hydroxy-methyl	Secondary hydroxyls	% Area of map	Hydroxy-methyl	Secondary hydroxyls
α-Kojibiose	*gggg* (0.0%)	*cc* (4.6%)	27.8	*gggg* (0.0%)	*cc* (0.0%)
	gggt (5.5%)	*cr'* (17.6%)		*gggt* (2.2%)	*cr'* (13.3%)
	gtgg (10.2%)	*r'c* (9.6%)		*gtgg* (14.4%)	*r'c* (4.4%)
	gtgt (84.3%)	*r'r'* (34.2%)		*gtgt* (83.3%)	*r'r'* (43.3%)
		rc (13.6%)			*rc* (14.5%)
		rr' (20.4%)			*rr'* (24.5%)
	Total representation of conformers:				
		14 of 24		9 of 24	
β-Kojibiose	*gggg* (0.3%)	*cc* (5.3%)	25.3	*gggg* (0.0%)	*cc* (1.2%)
	gggt (5.9%)	*cr* (21.6%)		*gggt* (0.0%)	*cr* (14.6%)
	gtgg (1.8%)	*r'c* (6.5%)		*gtgg* (1.2%)	*r'c* (6.1%)
	gtgt (92.0%)	*r'r* (34.9%)		*gtgt* (98.8%)	*r'r* (54.9%)
		rc (12.3%)			*rc* (8.5%)
		rr (19.4%)			*rr* (14.6%)
	Total representation of conformers:				
		15 of 24		7 of 24	
α-Nigerose	*gggg* (1.8%)	*cc* (21.6%)	29.0	*gggg* (1.1%)	*cc* (17.0%)
	gggt (6.2%)	*cr'* (8.6%)		*gggt* (3.2%)	*cr'* (5.3%)
	gtgg (24.7%)	*r'c* (21.9%)		*gtgg* (27.6%)	*r'c* (23.4%)
	gtgt (67.3%)	*r'r'* (23.2%)		*gtgt* (68.1%)	*r'r'* (27.7%)
		rc (11.1%)			*rc* (9.6%)
		rr' (13.6%)			*rr'* (17.0%)
	Total representation of conformers:				
		20 of 24		13 of 24	
β-Nigerose	*gggg* (2.8%)	*cc* (16.0%)	30.2	*gggg* (2.0%)	*cc* (14.3%)
	gggt (4.9%)	*cr* (15.7%)		*gggt* (4.1%)	*cr* (11.2%)
	gtgg (8.0%)	*r'c* (16.0%)		*gtgg* (12.2%)	*r'c* (19.4%)
	gtgt (84.3%)	*r'r* (11.1%)		*gtgt* (81.6%)	*r'r* (5.1%)
		rc (7.7%)			*rc* (7.1%)
		rr (33.3%)			*rr* (42.9%)
	Total representation of conformers:				
		17 of 24		13 of 24	
α-Maltose	*gggg* (1.2%)	*cc* (21.0%)	28.1	*gggg* (1.1%)	*cc* (17.6%)
	gggt (11.1%)	*cr'* (3.4%)		*gggt* (6.6%)	*cr'* (0.0%)
	gtgg (14.8%)	*r'c* (23.8%)		*gtgg* (25.3%)	*r'c* (23.1%)
	gtgt (72.9%)	*r'r'* (19.4%)		*gtgt* (67.0%)	*r'r'* (23.1%)
		rc (26.2%)			*rc* (30.7%)
		rr' (6.2%)			*rr'* (5.5%)
	Total representation of conformers:				
		19 of 24		10 of 24	
β-Maltose	*gggg* (0.6%)	*cc* (17.0%)	27.8	*gggg* (0.0%)	*cc* (8.9%)
	gggt (11.1%)	*cr* (7.7%)		*gggt* (7.8%)	*cr* (2.2%)
	gtgg (12.7%)	*r'c* (13.3%)		*gtgg* (18.9%)	*r'c* (7.8%)
	gtgt (75.6%)	*r'r* (38.6%)		*gtgt* (73.3%)	*r'r* (53.3%)
		rc (12.0%)			*rc* (16.7%)
		rr (11.4%)			*rr* (11.1%)
	Total representation of conformers:				
		17 of 24		11 of 24	

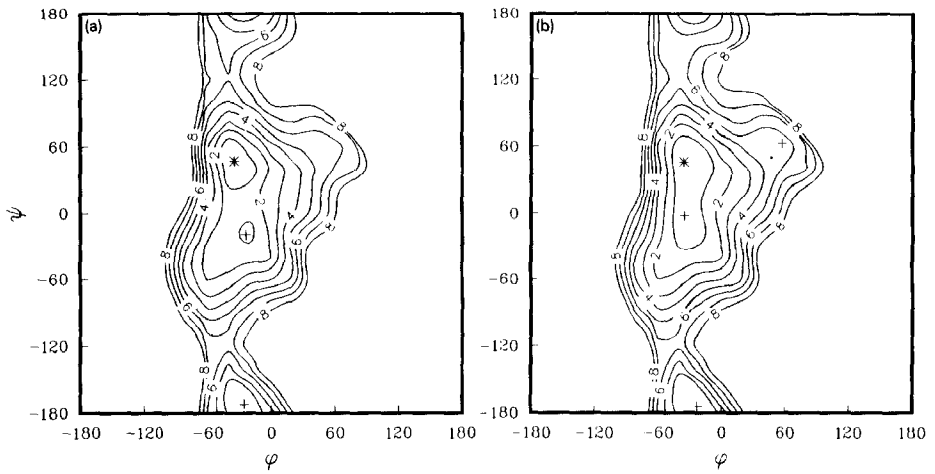

Fig. 5. MM3-generated relaxed-residue steric energy maps of α-nigerose (a) and β-nigerose (b). Contour lines are graduated in 1 kcal/mol increments above the global minimum; (*) global minimum; (+) other minima.

same result (Table IV). The large difference in this function for the two anomers appears to be due to the relatively high energy associated with the map region about the second minimum in β-kojibiose compared with the same region in α-kojibiose. A large difference for the same function is also found for (1 → 2)-β-linked sophorose anomers (work in progress).

α- and β-Nigerose.—The ϕ,ψ maps for α- and β-nigerose generated by MM3 are shown in Fig. 5, and the optimized minima are listed in Table II. All the nigerose minima but one are contained in a single low-energy region extending vertically across the map in the ψ-direction. The global minima for α- and β-nigerose are at $\phi,\psi = -35,47°$ and $\phi,\psi = -36,46°$, respectively. An inter-ring hydrogen bond is formed between O-5 and H(O-2′) in both anomeric forms, with oxygen-to-hydrogen distances of 0.1916 nm for α-nigerose and 0.1926 nm for β-nigerose. Selected bond lengths, valence angles, and torsional angles about the glycosidic linkages for the two global minima, showing few significant differences, are found in Table VI. The second lowest energy minimum for each anomer, located at $\phi,\psi = -24,-19°$ for α-nigerose and $\phi,\psi = -35,-2°$ for β-nigerose, has energy values within 1 kcal/mol of the global minimum. The third minimum is located in the staggered 180° region, with $\phi,\psi = -25,-172°$ for α-nigerose and $\phi,\psi = -23,-174°$ for β-nigerose. A plateau region occurs at approximately 60, 60° on both plots, as it does for the two kojibiose anomers, but a minimum could be found for only β-kojibiose, and only by using the full-matrix minimization method. The Boltzmann-averaged energy is lower for β-nigerose (Table IV). NMR spectroscopy of nigerose in deuterium oxide finds a higher equilibrium concentration of β-nigerose, in agreement with our vacuum-based calculations[23]. Nigerose equilibrium was also investigated in water[25] and in pyridine[26] by gas–liquid chromatog-

TABLE VI

Selected MM3-generated bond lengths, valence angles, and torsional angles for the global minima of α- and β-nigerose

	α-Nigerose	β-Nigerose
	Bond lengths (nm)	
C-1–C-2	0.1528	0.1528
C-1–O-1	0.1419	0.1419
C-1–O-5	0.1422	0.1422
C-5–O-5	0.1426	0.1426
C-1′–O-1′	0.1438	0.1427
C-1′–O-5′	0.1407	0.1414
C-2′–C-3′	0.1531	0.1534
C-3′–C-4′	0.1531	0.1532
C-3′–O-1	0.1427	0.1428
C-5′–O-5′	0.1424	0.1422
	Valence angles (degrees)	
C-1–O-1–C-3′	115.8	115.8
C-1–O-5–C-5	114.9	115.0
C-2–C-1–O-1	108.9	108.9
C-2–C-1–O-5	108.5	108.4
O-1–C-1–O-5	111.2	111.4
C-1′–O-5′–C-5′	114.2	112.2
C-2′–C-1′–O-1′	110.2	108.2
C-2′–C-1′–O-5′	110.0	109.0
C-2′–C-3′–O-1	111.3	111.1
C-2′–C-3′–C-4′	107.9	108.8
C-4′–C-3′–O-1	105.2	105.3
O-1′–C-1′–O-5′	110.0	107.1
	Torsional angles (degrees)	
H-1–C-1–O-1–C-3′	−34.8	−36.0
C-1–O-1–C-3′–H-3′	47.4	46.3
C-1–O-1–C-3′–C-2′	−77.2	−77.6
C-1–O-1–C-3′–C-4′	166.3	164.8
C-2–C-1–O-1–C-3′	−153.8	−154.8
C-2–C-1–O-5–C-5	−60.0	−59.9
C-5–O-5–C-1–O-1	59.8	60.0
O-5–C-1–O-1–C-3′	86.7	85.6

chromatography, but the anomeric peak assignments were not determined. The NMR results supported by our computational energies suggest that the dominant nigerose peak of Nikolov and Reilly[26] (peak 2) represents the β anomer.

Maps of the contributing initial conformers of nigerose are shown in Fig. 6. Most of the starting conformations contribute at least one point to the final maps (20 and 17 of 24, respectively, for α- and β-nigerose) and many occur within the 8 kcal/mol region (13 of 24 for each anomer). The dominant hydroxymethyl orientation is *gtgt*, although the *gtgg* conformation is also well represented in α-nigerose (Table V). A fairly even distribution among *cc*, *r′c*, *r′r′*, and *rr′* orientations is found in α-nigerose, while the *rr* orientation is most important in β-nigerose. The

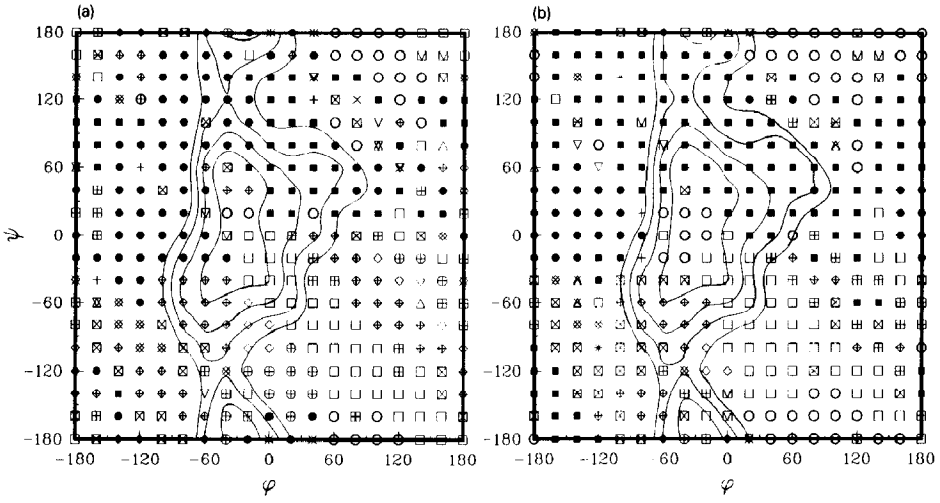

Fig. 6. Distribution of the starting conformers that contribute to the final relaxed-residue maps of α-nigerose (a) and β-nigerose (b). Starting conformers are: *ggggcc* (✳); *ggggcx* (⊠); *ggggr'c* (⊙); *ggggr'x* (⧓); *ggggrc* (⧖); *gggtcc* (⊗); *gggtcx* (⊠); *gggtr'x* (+); *gggtrc* (×); *gggtrx* (∗); *gtggcc* (⊕); *gtggcx* (⊠); *gtggr'c* (⊕); *gtggr'x* (▽); *gtggrc* (◇); *gtggrx* (△); *gtgtcc* (□); *gtgtcx* (○); *gtgtr'c* (⊠); *gtgtr'x* (●); *gtgtrc* (⊞); *gtgtrx* (■). For the reducing ring secondary hydroxyl orientation, *x* represents *r'* for α-nigerose and *r* for β-nigerose. Contour lines are graduated in 2 kcal/mol increments above the global minimum.

8 kcal/mol energy contour line encloses a larger portion of the map space for β-nigerose, indicating it has slightly more conformational freedom about its glycosidic linkage than does α-nigerose. The partition function (Table IV) suggests the same result.

α- and β-Maltose.—MM3-generated maps for α- and β-maltose are shown in Fig. 7. Two distinct low-energy regions appear on each map. The dominant region for each anomer, containing the lowest two of the three α-maltose minima and the lowest three of the four β-maltose minima, extends diagonally from $\phi,\psi = -90, -90°$ to $\phi,\psi = 0,60°$. The lowest minima are at $\phi,\psi = -23, -22°$ for α-maltose and $\phi,\psi = -54, -47°$ for β-maltose. A hydrogen bond exists between O-2 and H(O-3') for α-maltose with an oxygen-to-hydrogen distance of 0.2150 nm, which is not as strong as the inter-ring hydrogen bonds formed for some of the low-energy conformers of kojibiose and nigerose. Selected geometric properties for the atoms about the glycosidic bonds and anomeric regions of the two global minima, showing few significant differences except in torsional angles, are shown in Table VII. An additional minimum, only slightly higher in energy, is found within the 1 kcal/mol contour line for each anomer (Fig. 7 and Table II). The locations of these second minima are essentially the reverse of those of the global minima, at $\phi,\psi = -55, -48°$ for α-maltose and $\phi,\psi = -28, -28°$ for β-maltose. A third shallow β-maltose minimum occurs at $\phi,\psi = 1,24°$. A second low-energy region exists, with ψ staggered about the 180° potential well, holding minima at ϕ,

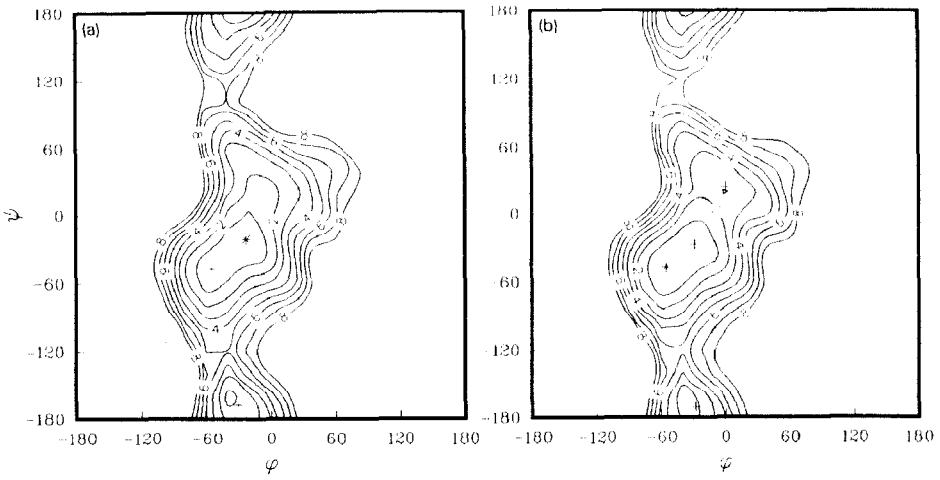

Fig. 7. MM3-generated relaxed-residue steric energy maps of α-maltose (a) and β-maltose (b). Contour lines are graduated in 1 kcal/mol increments above the global minimum: (*) global minimum; (+) other minima.

$\psi = -31, -168°$ for α-maltose and at $\phi,\psi = -28, -170°$ for β-maltose. The energy differences between these minima and the global minima are less than 2 to 3 kcal/mol for both anomers, although the increase in energy required to reach this region from the global minima is more than 5 kcal/mol. The Boltzmann-averaged energies suggest that β-maltose would be the dominant isomer in the gas phase, as is found experimentally in deuterium oxide[23], in water[24,25], and in pyridine[26].

The starting conformations that yield the lowest energies at each point are shown in Fig. 8. Some differences are found in the populations of starting conformers that contribute final points within the low-energy region of the maps for α- and β-maltose (Fig. 8 and Table V). The *gtgt* orientation of the hydroxymethyl groups dominates in both maltose anomers, as it does for kojibiose and nigerose, although mixed hydroxymethyl orientations (*gtgg* or *gggt*) are important. Starting secondary hydroxyl orientations in α-maltose are predominantly *rc*, *r'c*, *cc*, and *r'r'*, while in β-maltose *r'r* is most prevalent. The areas enclosed by the 8 kcal/mol contour line are almost identical, but suggest that slightly more freedom is afforded α-maltose. In contrast, the partition coefficients indicate that β-maltose occupies more conformational space (Table IV). The discrepancy shows that isoenergy contour lines may not be the most accurate indications of conformational freedom.

Comparisons among disaccharides.—The general map characteristics for the six disaccharides studied are similar. A single trough of low-energy conformers is found in the ψ-direction, indicating freedom of rotation about this equatorial bond. The troughs all have their global minima at φ values between −60 and 0°, the location being an expression of the exo-anomeric effect. Previously published

TABLE VII

Selected MM3-generated bond lengths, valence angles, and torsional angles for the global minima of α- and β-maltose compared with other computational studies and crystallographic data

Bonds	α-Maltose		β-Maltose		
	MM3 model [a]	Anhydrous structure [b]	MM3 model [a]	Mono-hydrate structure [c]	Methyl β-malto-pyranoside monohydrate structure [d]
	Bond lengths (nm)				
C-1–C-2	0.1525	0.1511	0.1528	0.1535	0.1514
C-1–O-1	0.1423	0.1415	0.1418	0.1414	0.1416
C-1–O-5	0.1421	0.1420	0.1420	0.1403	0.1408
C-5–O-5	0.1427	0.1433	0.1425	0.1434	0.1440
O-1–C-4′	0.1428	0.1437	0.1427	0.1419	0.1438
C-1′–O-1′	0.1438	0.1375	0.1420	0.1389	0.1375
C-1′–O-5′	0.1409	0.1433	0.1424	0.1419	0.1427
C-3′–C-4′	0.1531	0.1523	0.1536	0.1526	0.1513
C-4′–C-5′	0.1533	0.1530	0.1538	0.1534	0.1512
C-5′–O-5′	0.1426	0.1423	0.1422	0.1423	0.1430
	Valence angles (degrees)				
C-1–O-1–C-4′	113.7	120.1	116.6	117.8	117.6
C-1–O-5–C-5	114.9	113.9	115.5	113.8	114.7
C-2–C-1–O-1	109.8	109.7	108.1	108.8	107.8
C-2–C-1–O-5	109.3	109.1	108.8	110.5	110.9
O-1–C-1–O-5	110.1	107.3	112.3	110.7	111.5
C-1′–O-5′–C-5′	114.7	113.6	112.0	112.7	111.5
C-2′–C-1′–O-1′	110.3	112.0	107.4	108.3	108.9
C-2′–C-1′–O-5′	109.5	113.2	107.8	110.2	110.3
C-3′–C-4′–O-1	107.5	105.6	110.7	108.0	107.9
C-3′–C-4′–C-5′	108.7	112.2	109.4	109.2	111.0
C-5′–C-4′–O-1	108.0	107.3	105.2	110.9	111.1
O-1′–C-1′–O-5′	109.9	106.0	108.6	108.2	107.1
	Torsional angles (degrees)				
H-1–C-1–O-1–C-4′	−22.7	−4.7	−54.3	4.8	−9.1
C-1–O-1–C-4′–H-4′	−21.7	2.1	−47.4	13.3	10.2
C-1–O-1–C-4′–C-3′	100.3	122.2	76.1	132.8	129.2
C-1–O-1–C-4′–C-5′	−142.5	−118.0	−165.8	−107.7	−108.9
C-2–C-1–O-1–C-4′	−142.3	−125.5	−172.2	−116.7	−128.2
C-5–O-5–C-1–C-2	−58.9	−63.9	−58.8	−60.6	−56.2
O-5–C-1–C-2–C-3	55.3	59.7	54.5	57.4	56.2
O-5–C-1–O-1–C-4′	97.4	116.1	67.8	121.7	110.0
	Intramolecular distances (nm)				
O-2 ··· O-3′	0.3048	0.2770		0.2789	0.2825
O-2 ··· H-3′	0.2150	0.2060			
H-2 ··· O-3′				0.1835	0.1862

[a] This work. [b] Ref. 28. [c] Ref. 36. [d] Ref. 37.

relaxed maps of α,β-trehalose[10] (using MM3), of mannose disaccharides[21,22] (using MM2CARB), and of maltose[2–4] [using MM2CARB and MM2(85)] also show this same property. An additional maltose map[1] (using CHARMM), which is not

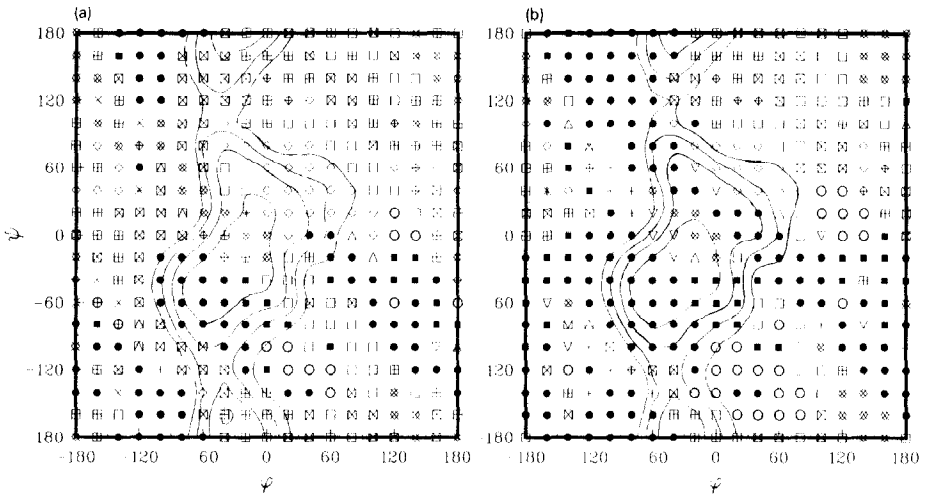

Fig. 8. Distribution of the starting conformers that contribute to the final relaxed-residue maps of α-maltose (a) and β-maltose (b). Starting conformers are: *ggggcc* (✳); *ggggr'c* (⊕); *ggggr'x* (✴); *gggtcc* (⊗); *gggtcx* (☒); *gggtr'c* (▨); *gggtr'x* (+); *ggtrc* (×); *ggtrx* (✳); *gtggcc* (⊕); *gtggr'c* (✣); *gtggr'x* (▽); *gtggrc* (◇); *gtggrx* (△); *gtgtcc* (□); *gtgtcx* (○); *gtgtr'c* (⊠); *gtgtr'x* (●); *gtgtrc* (⊞); *gtgtrx* (■). For the reducing ring secondary hydroxyl orientation, *x* represents *r'* for the α-maltose and *r* for β-maltose. Contour lines are graduated in 2 kcal/mol increments above the global minimum.

parameterized for anomeric effects, centers this trough in an eclipsed configuration near $\phi = 0°$.

The lowest 3 kcal/mol regions are notably different in the different carbohydrate isomers. For α-kojibiose, the trough region is distinctly separated into two low-energy regions, one located to each side of the eclipsed $\psi = 0°$ conformation. For β-kojibiose, the two regions exist, but one is not as pronounced as the other, with energies about 2 kcal/mol higher. For the nigerose anomers, the energy barrier between these two minimum regions is lower than for the corresponding kojibiose anomers, and the minima in the negative ψ-region are shifted more toward the eclipsed conformation (toward 0°). Finally, for maltose these two low-energy wells form a single low-energy area, although separate minima with similar energies occur. Sathyanarayana and Rao found the global minima for α-kojibiose and α-nigerose in the positive ψ-region and the global minimum for α-maltose in the negative ψ-region[9]. Relaxed MM3 maps support these same results except for α-kojibiose, where the minimum with the second lowest energy, which differs from the global minimum by less than 0.2 kcal/mol, is the one with a positive ψ. The second low-energy region in maltose is favored compared to those of kojibiose and nigerose because the hydroxymethyl group on the reducing ring is farther away from the ring oxygen atom on the nonreducing ring. In addition, its conformation is stabilized by the hydrogen bond between the hydroxyl groups attached to C-2 and C-3'.

The 8 kcal/mol contour line encompasses a slightly higher percentage of ϕ,ψ space for the two nigerose anomers. This may occur because the glycosidic linkage

in nigerose is more distant both from the anomeric region and from the bulky 5′-hydroxymethyl group. For α anomers, the degree of flexibility, considering the area within the 8 kcal/mol contour line, is in order of linkage $(1 \rightarrow 3) > (1 \rightarrow 4) > (1 \rightarrow 2)$. The equivalent order determined from the molecular partition function is $(1 \rightarrow 3) > (1 \rightarrow 2) > (1 \rightarrow 4)$. This is in contrast with the early results based on contact distance calculations of Sathyanarayana and Rao[9] that suggest that α-kojibiose has a greater degree of conformational freedom than α-nigerose and then α-maltose $[(1 \rightarrow 2) > (1 \rightarrow 3) > (1 \rightarrow 4)]$. For β anomers, the degree of flexibility is $(1 \rightarrow 3) > (1 \rightarrow 4) > (1 \rightarrow 2)$, both from areas enclosed within the 8 kcal/mol contour line and from the partition function.

The Boltzmann-averaged map energies are in the order kojibiose < nigerose < maltose. An equilibrium concentration of a mixture of these disaccharides would then be the reverse (maltose < nigerose < kojibiose), assuming that other conformation-dependent components of the free energy can be ignored. Experimentally derived equilibrium constants, defined as [disaccharide][water]/[D-glucose]^2, for the glucoamylase-catalyzed formation of the α-linked D-glucosyl disaccharides from D-glucose and water are $K_{\alpha,\beta\text{-trehalose}} \ll K_{\text{maltose}} < K_{\text{nigerose}} < K_{\text{kojibiose}} \ll K_{\text{isomaltose}}$[27]. Isomaltose [$\alpha$-D-glucopyranosyl-(1 → 6)-D-glucose], not studied here, should yield lower MM3 energies and, therefore, a higher equilibrium concentration because the extra degree of rotational freedom at its glycosidic linkage reduces steric effects between the rings. MM3 energies for α,β-trehalose, reported in a previous study[10], are low in relation to this ordering. This discrepancy is difficult to explain, but may be related to the unusual dual anomeric effects that are unique to this molecule in the axially–equatorially linked D-glucosyl disaccharide series.

Comparisons with tetrahydropyran analogues.—Previous work has shown that adiabatic energy maps of the three trehaloses are strikingly similar to analogous maps of their 6-methyltetrahydropyran analogues [10]. This suggests that exo-cyclic factors, e.g., hydrogen bonding, are of secondary importance in determining conformational flexibility in some environments, although such effects may be important in stabilizing preferred conformations. Similar energy maps generated by MM3 at $\varepsilon = 4.0$ for the analogues of kojibiose [axially–equatorially linked 3-(6-methyltetrahydropyran-2-yloxy)-6-methyltetrahydropyran], nigerose [axially–equatorially linked 4-(6-methyltetrahydropyran-2-yloxy)-6-methyltetrahydropyran], and maltose [axially–equatorially linked 5-(6-methyltetrahydropyran-2-yloxy)-6-methyltetrahydropyran] are shown in Fig. 9, with the localized minima given in Table VIII. It is clear that the general character of maps of axially–equatorially linked disaccharides is not greatly influenced by removal of hydroxyl groups from them. This suggests that hydrogen bonding is not a primary factor in determining favorable disaccharide conformations in media of elevated dielectric constant. The maps for the tetrahydropyran analogues of kojibiose and nigerose are almost identical to each other and are different from that of the maltose analogue, indicating that the presence of a bulky methyl or hydroxymethyl group on the

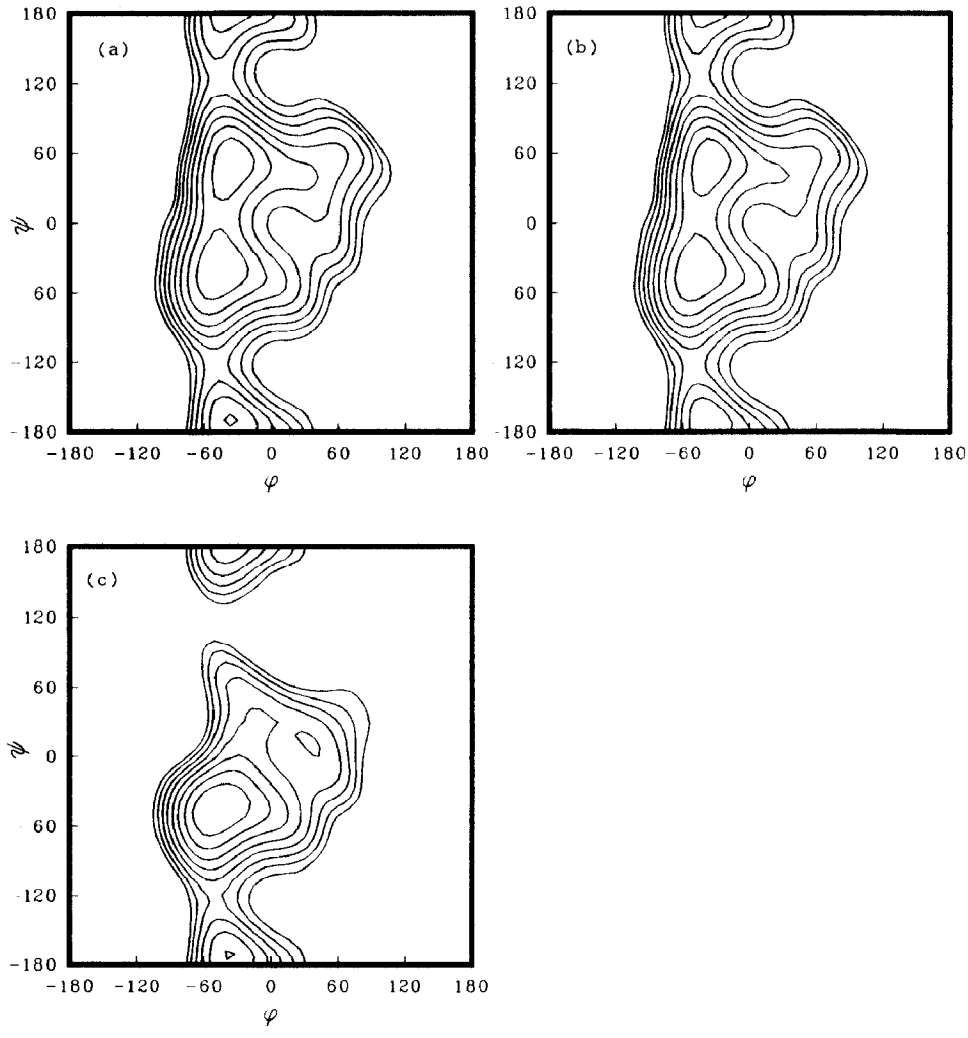

Fig. 9. MM3-generated relaxed-residue steric energy maps of 3-(6-methyltetrahydropyran-2-yloxy)-6-methyltetrahydropyran (a), 4-(6-methyltetrahydropyran-2-yloxy)-6-methyltetrahydropyran (b), and 5-(6-methyltetrahydropyran-2-yloxy)-6-methyltetrahydropyran (c).

carbon atom next to the glycosidic linkage does influence disaccharide conformational freedom. All low-energy wells found on the disaccharide maps are reproduced on the analogue maps, but the plateau regions are not as well defined. The Boltzmann-averaged energy values are in the order nigerose analogue < kojibiose analogue < maltose analogue, different than those for the disaccharides, and appear to increase as the analogue reducing-ring oxygen atom is moved closer to interring bonds.

Comparisons with previous maps and crystal structures.—Several groups have presented relaxed-residue maltose maps using different computational methods, the earliest using a carbohydrate-modified CHARMM function[1] and MM2CARB[2].

TABLE VIII

Steric energy minima for MM3-generated relaxed-residue analysis of the 6-methyltetrahydropyran analogues of kojibiose, nigerose, and maltose

Structure	Location of minimum		Relaxed energy (kcal/mol)
	ϕ	ψ	
Axially–equatorially linked	−46.4	−38.8	20.12
3-(6-methyltetrahydropyran-2-yloxy)-	−35.7	51.9	20.29
6-methyltetrahydropyran	−37.1	−169.7	23.01
Axially–equatorially linked	−46.7	−44.7	19.31
4-(6-methyltetrahydropyran-2-yloxy)-	−36.1	52.1	20.24
6-methyltetrahydropyran	−37.3	−169.6	23.02
Axially–equatorially linked	−47.7	−44.7	20.31
5-(6-methyltetrahydropyran-2-yloxy)	−36.8	−171.5	23.26
6-methyltetrahydropyran	37.5	9.4	24.27

Several initial conformers were used to generate these maps, including *tg* orientations of the hydroxymethyl groups, not studied here. These maps based on other force fields have more low-energy regions than appear on maps presented here. The CHARMM map of β-maltose has five distinct regions separated by barriers of 1 kcal/mol or more[1], while the MM2CARB map has at least three areas containing minima that are separated by 1 kcal/mol barriers, with six minima within these regions[2]. An MM2(85) α-maltose map by French with a single initial conformer also has three regions containing minima[3]. In contrast, the α- and β-maltose maps presented here have only two distinct regions. There are two possible reasons for the differences. First, they may be caused by the force field itself. For cellobiose, comparable maps based on MM3 have yielded lower energy barriers between minima than maps based on MM2(85) (work in progress), and similar results would be expected for other force fields. Second, the systematic use of several different conformers (24 in this study) may allow lower energy values to be found and result in flatter energy profiles than would be generated from considering only a few conformers. It is probable that both factors influence the final maps. Using a CHARMM-based potential function, Ha et al. found that the starting chair orientation of the reducing ring of β-maltose could be converted to a boat form during development of their adiabatic map (Fig. 3, ref. 1). These ring structure conversions were found in three areas of the map that tended to correspond to high-energy regions. We studied several final grid-point structures from these regions of the MM3 β-maltose map but did not find the same transformations, although the chair ring angles were sometimes distorted by 20° from the staggered chair orientations of $\pm 60°$. Although this does not prove that other ring conformations do not contribute to adiabatic disaccharide maps, it does indicate that these conversions occur less frequently within MM3 than within CHARMM-based potential functions.

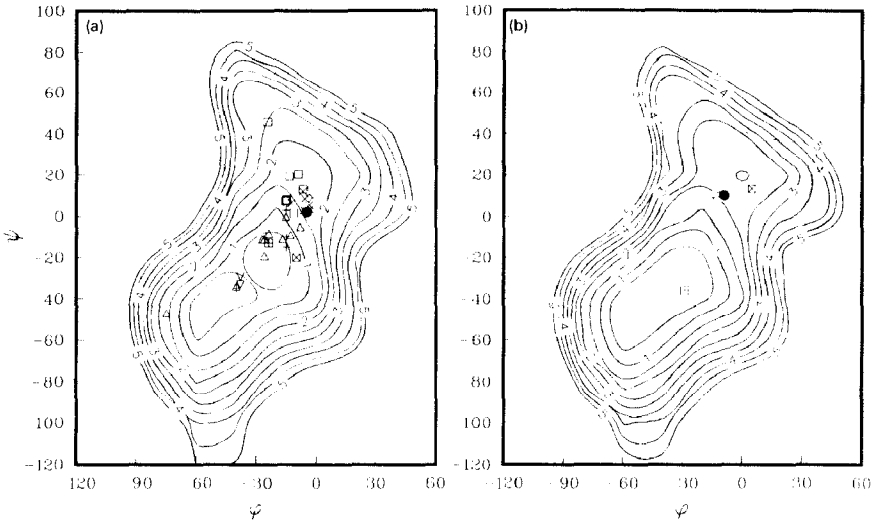

Fig. 10. Comparison of an MM3-generated relaxed-residue steric energy map of maltose with selected known crystal structures for maltose, malto-oligosaccharides, and related structures. α-Maltose map (a) plus crystal structures: α-maltose[28] (●); phenyl α-maltoside[29] (⊠); panose[30] (⊞); methyl α-maltotrioside tetrahydrate[31] (▽); *p*-nitrophenyl α-maltohexaoxide[32] (△); α-cyclomaltohexaose hexahydrate[33] (□); maltoheptaose[34] (+); cyclomaltoheptaose hydrate[35] (×). β-Maltose map (b) plus crystal structures: β-maltose monohydrate[36] (⊠; methyl β-maltoside monohydrate[37] (●); β-maltose octaacetate[38] (⊞).

In order to test whether MM3 represents an improvement over previous methods, the ϕ, ψ values of a number of maltose-containing crystal structures are plotted on maps covering the low-energy region of each anomer (Fig. 10). A similar comparison made with an MM2(85) map using only one starting geometry (*gggg*) indicated that all the crystal structures fell within 4 kcal/mol of the modeling minimum[3]. The same crystal structures have been used in this study, which were chosen to show the broadest range of values of the glycosidic torsional angles found in crystals. The MM3 model appears to be an improvement, with all the crystal structures falling within 2.7 kcal/mol. The two most extreme points, 2.7 and 2.5 kcal/mol from the calculated global minimum of α-maltose, are from complex oligosaccharides, where intermolecular packing forces may be larger. Although the crystal points are not clustered evenly around the global minima, the crescent-shaped low-energy regions of ϕ,ψ space where the crystal structures are found are clearly delineated on the MM3 maps. However MM2CARB[2] and MM2(85)[3,4] maps of α-maltose, which have minima at positive values of ϕ, have low-energy regions in which the crystal structures of α-maltose are more centered than in the MM3 map, which does not have an analogous minimum.

A comparison of structural parameters from crystallographic results on maltose disaccharides and simple derivatives with the global minima derived from MM3 is presented in Table VII. MM3-predicted bond lengths and valence angles are in good agreement with those found from crystallography. MM3 does underestimate

the C-1–O-1–C-4′ glycosidic valence angle, but work on other disaccharides using MM2(85) has shown that the energy values are not strongly affected by this angle[39], which may explain the difference. There are variations in the torsional angles, consistent with the differences in map locations of the crystal structures and the MM3-generated global minimum. MM3 does reproduce the O-2 to O-3′ intramolecular hydrogen bond, although for β-maltose it is found on the second low-energy minima. The low-energy initial conformer structures yielding the minima stabilized by inter-ring hydrogen bonds are different for the two anomeric forms of maltose. For α-maltose, the global minimum is derived from a *cc* orientation of the secondary hydroxyl groups, and it is the H(O-3′) hydrogen atom that is involved in the hydrogen bond. In contrast, an *rr* initial conformer contributes the second minimum structure for β-maltose, and the hydrogen donor in this case is the H(O-2) atom. Similarly, in the α-maltose crystal the O-3′ oxygen atom donates the hydrogen, while in both β-maltose structures the hydrogen atom is donated by the O-2 oxygen atom.

CONCLUSIONS

MM3-based relaxed-residue maps of both anomeric forms of kojibiose, nigerose, and maltose have been computed. The overall characteristics of the maps are similar, illustrating the importance of the axial–equatorial glycosidic linkage in determining conformation. This was confirmed by computing energy surfaces for 6-methyltetrahydropyran analogues of all three disaccharides. Within the low-energy region (< 8 kcal/mol above the global minimum), the maps exhibit differences that must be related to the positioning of the glycosidic bonds relative to the anomeric region and to the hydroxymethyl group. Agreement of the maltose results with crystallographic data on maltosyl-containing molecules is at least equal to that previously reported.

REFERENCES

1 S.N. Ha, J. Madsen, and J.W. Brady, *Biopolymers*, 27 (1988) 1927–1952.
2 V. Tran, A. Buleon, A. Imberty, and S. Pérez, *Biopolymers*, 28 (1989) 679–690.
3 A.D. French, *Carbohydr. Res.*, 188 (1989) 206–211.
4 A.D. French and J.W. Brady, *ACS Symp. Ser.*, 430 (1990) 1–19.
5 A.D. French, *Biopolymers*, 27 (1988) 1519–1525.
6 A.D. French, in C. Schuerch (Ed.), *Cellulose and Wood—Chemistry and Technology*, Wiley, New York, 1989, pp. 103–118.
7 A.D. French, V.H. Tran, and S. Pérez, *ACS Symp. Ser.*, 430 (1990) 191–211.
8 B.K. Sathyanarayana and V.S.R. Rao, *Biopolymers*, 10 (1971) 1605–1615.
9 B.K. Sathyanarayana and V.S.R. Rao, *Biopolymers*, 11 (1972) 1379–1394.
10 M.K. Dowd, P.J. Reilly, and A.D. French, *J. Comput. Chem.*, 13 (1992) 102–114.
11 N.L. Allinger, Y.H. Yuh, and J.H. Lii, *J. Am. Chem. Soc.*, 111 (1989) 8551–8566.
12 J.H. Lii and N.L. Allinger, *J. Am. Chem. Soc.*, 111 (1989) 8566–8575.
13 N.L. Allinger, M. Rahman, and J.H. Lii, *J. Am. Chem. Soc.*, 112 (1990) 8293–8307.
14 N.L. Allinger, *J. Am. Chem. Soc.*, 99 (1977) 8127–8134.

15 K. Gundertofte, J. Palm, I. Pettersson, and A. Stamvik, *J. Comput. Chem.*, 12 (1991) 200–208.
16 A.D. French, R.J. Rowland, and N.L. Allinger, *ACS Symp. Ser.*, 430 (1990) 120–140.
17 R.H. Marchessault and S. Pérez, *Biopolymers*, 18 (1979) 2369–2374.
18 A. De Bruyn and M. Anteunis, *Carbohydr. Res.*, 47 (1976) 311–314.
19 Y. Nishida, H. Ohrui, and H. Meguro, *Tetrahedron Lett.*, 25 (1984) 1575–1578.
20 I. Tvaroška and L. Václavík, *Carbohydr. Res.*, 160 (1987) 137–149.
21 A. Imberty, V. Tran, and S. Pérez, *J. Comput. Chem.*, 11 (1989) 205–216.
22 J.P. Carver, D. Mandel, S.W. Michnick, A. Imberty, and J.W. Brady, *ACS Symp. Ser.*, 430 (1990) 266–280.
23 T. Usui, M. Yokoyama, N. Yamaoka, K. Matsuda, K. Tuzimura, H. Sugiyama, and S. Seto, *Carbohydr. Res.*, 33 (1974) 105–116.
24 J. Haverkamp, J.P. Kamerling, and J.F.G. Vliegenthart, *J. Chromatogr.*, 59 (1971) 281–287.
25 T. Toba and S. Adachi, *J. Chromatogr.*, 135 (1977) 411–417.
26 Z.L. Nikolov and P.J. Reilly, *J. Chromatogr.*, 254 (1983) 157–162.
27 Z.L. Nikolov, M.M. Meagher, and P.J. Reilly, *Biotechnol. Bioeng.*, 34 (1989) 694–704.
28 F. Takusagawa and R.A. Jacobson, *Acta Crystallogr., Sect. B*, 34 (1978) 213–218.
29 I. Tanaka, N. Tanaka, T. Ashida, and M. Kakudo, *Acta Crystallogr., Sect. B*, 32 (1976) 155–160.
30 A. Imberty and S. Pérez, *Carbohydr. Res.*, 181 (1988) 41–55.
31 W. Pangborn, D. Langs, and S. Pérez, *Intl. J. Biol. Macromol.*, 7 (1985) 363–369.
32 W. Hinrichs and W. Saenger, *J. Am. Chem. Soc.*, 112 (1990) 2789–2796.
33 K. Linder and W. Saenger, *Acta Crystallogr., Sect. B*, 38 (1982) 203–210.
34 E. Goldsmith, S. Sprang, and R. Fletterick, *J. Mol. Biol.*, 156 (1982) 411–427.
35 J.A. Hamilton and M.N. Sabesan, *Carbohydr. Res.*, 102 (1982) 31–46.
36 M.E. Gress and G.A. Jeffrey, *Acta Crystallogr., Sect. B*, 33 (1977) 2490–2495.
37 S.S.C. Chu and G.A. Jeffrey, *Acta Crystallogr., Sect. B*, 23 (1967) 1038–1049.
38 F. Brisse, R.H. Marchessault, S. Pérez, and P. Zugenmaier, *J. Am. Chem. Soc.*, 104 (1982) 7470–7476.
39 C.H. du Penhoat, A. Imberty, N. Roques, V. Michon, J. Mentech, G. Descotes, and S. Pérez, *J. Am. Chem. Soc.*, 113 (1991) 3720–3727.